# Oscillations and multistability in two semiconductor ring lasers coupled by a single waveguide

W. Coomans,* G. Van der Sande, and L. Gelens†
*Applied Physics Research Group (APHY), Vrije Universiteit Brussel, Pleinlaan 2, B-1050 Brussel, Belgium*
(Received 7 July 2013; published 5 September 2013)

We theoretically study the dynamical behavior of semiconductor ring lasers coupled by a single bus waveguide, both when weakly coupled and when strongly coupled. We provide a detailed analysis of the multistable landscape in the coupled system, analyze the stability of all solutions, and relate the internal dynamics in the individual lasers to the field effectively measured at the output of the waveguide. We show that coupling phases close to $\pi/2$ generally promote instabilities. Finally, our analysis enables us to discuss the advantages and disadvantages for optical memory operation of coupled semiconductor ring lasers versus solitary ones.

DOI: 10.1103/PhysRevA.88.033813 PACS number(s): 42.55.Px, 42.65.Sf, 42.60.Mi

Semiconductor ring lasers (SRLs) are semiconductor lasers where the laser cavity consists of a ring-shaped waveguide. SRLs can generate light in two counterpropagating directions referred to as the clockwise (CW) and the counterclockwise (CCW) modes. Bistability between both directional modes has been demonstrated, allowing us to encode digital information in the direction of emission of SRLs [1]. This bistable operation allows SRLs to be used in systems for all-optical switching and as all-optical memories, both in solitary [2–4] and coupled [1,5–8] configurations. Moreover, SRLs are highly integrable and scalable [9], making them ideal candidates for key components in photonic integrated circuits.

One of the seminal works reporting on the potential of SRLs as optical memories is the paper by Hill *et al.* [1]. To demonstrate fast optical flip-flop operation, the authors fabricated two SRLs coupled by a single waveguide, rather than a solitary SRL. Nevertheless, the literature shows that a single SRL can also function perfectly as an all-optical memory [4]. This raises the question as to whether coupling two SRLs to realize a single optical memory has any advantage over using a solitary SRL, taking into account the obvious disadvantage of a doubled footprint and power consumption.

In a broader context, coupled lasers received a lot of attention in recent years, e.g., the dynamics of coupled semiconductor lasers by a passive resonator with [10–12] or without delay [13], coupled photonic crystal microcavities [14], laterally coupled semiconductor lasers [15], and microdisk photonic molecule lasers [5,16,17] have recently been investigated. This interest in coupled lasers is, among others, raised by the recent application-driven technological progress, allowing for the fabrication of photonic integrated circuits comprising of many active and passive structures [18]. A more fundamental interest in coupled, or even whole networks of, nonlinear oscillators exist, where coupled lasers can provide a toy model for studying general synchronization properties of coupled nonlinear oscillators [19–24]. Also, coupling two excitable (asymmetric) SRLs to mimic neural functionality by transferring pulses is possible and of interest [25,26].

In a recent experimental investigation of coupled SRLs, we have demonstrated that coupling between SRLs can destabilize the system by exciting relaxation oscillations, similar to an optically injected laser system [8]. In this article, we will pursue a more in-depth theoretical investigation of dynamics induced by the coupling. Similar as in Ref. [8], we will consider the single waveguide coupling configuration as shown in Fig. 1. The coupling provides the system with two extra degrees of freedom, the coupling strength and the physical distance between the SRLs. The latter is taken into account by defining a coupling phase equal to the optical phase difference accumulated when traveling from one SRL to another. However, explicit time-delay effects in the coupling (because of the finite traveling time between the lasers) are neglected.

In Sec. I, we introduce the model equations used throughout the paper. Sections II and III are devoted to a careful bifurcation analysis of the existence and stability of various solutions existing in the coupled laser system. We distinguish between two regions of operations: a weak-coupling region (see Sec. II) and a strong-coupling region (see Sec. III). In each case, we study the influence of pump current, coupling phase, and coupling strength on the stability and power suppression ratio of the various lasing states. Finally, in Sec. IV, we discuss the similarities and differences in observed dynamics of weakly or strongly coupled SRLs. Moreover, we relate our results to previous experimental results and consider whether either coupled or solitary SRLs are more suitable to be used as optical memory components.

## I. MODEL

To model the single-waveguide-coupled SRLs, we use the rate-equation model for a solitary SRL (see, e.g., [3,27]) and modify it to comply with our asymmetric coupling configuration, as illustrated in Fig. 1. Other coupling configurations that maintain the symmetry properties of the solitary SRL could be considered as well, such as double-waveguide coupling and point coupling. Here, we focus on single-waveguide coupling as it has been suggested for use as an optical memory in Ref. [1]. For each SRL X (X = {A,B}), the model consists of two slowly varying complex envelopes of the counterpropagating waves $E_{1X}$ (CW) and $E_{2X}$ (CCW) and a third equation for the carrier population inversion $N_X$:

$$\dot{E}_{1A} = \kappa(1+i\alpha)[g_{1A}N_A - 1]E_{1A} - ke^{i\phi_k}E_{2A}, \tag{1a}$$

$$\dot{E}_{2A} = \kappa(1+i\alpha)[g_{2A}N_A - 1]E_{2A} - ke^{i\phi_k}E_{1A} - k_c e^{i\phi_c}E_{2B}, \tag{1b}$$

*Present address: Alcatel-Lucent Bell Labs, Copernicuslaan 50, 2018 Antwerp, Belgium.
†lgelens@vub.ac.be

 

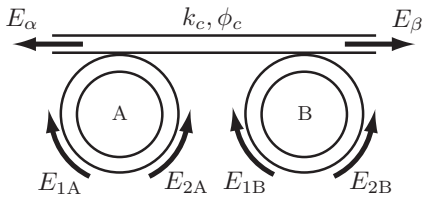


FIG. 1. The counterpropagating fields in SRL A (B) are referred to as $E_{1A}$ and $E_{2A}$ ($E_{1B}$ and $E_{2B}$). The total field at the left (right) output is referred to as $E_\alpha$ ($E_\beta$). The coupling amplitude is referred to as $k_c$, and the coupling phase as $\phi_c$.

$$\dot{E}_{1B} = \kappa(1+i\alpha)[g_{1B}N_B - 1]E_{1B} - ke^{i\phi_k}E_{2B} - k_c e^{i\phi_c}E_{1A}, \tag{1c}$$

$$\dot{E}_{2B} = \kappa(1+i\alpha)[g_{2B}N_B - 1]E_{2B} - ke^{i\phi_k}E_{1B}, \tag{1d}$$

$$\dot{N}_A = \gamma[\mu - N_A - g_{1A}N_A|E_{1A}|^2 - g_{2A}N_A|E_{2A}|^2], \tag{1e}$$

$$\dot{N}_B = \gamma[\mu - N_B - g_{1B}N_B|E_{1B}|^2 - g_{2B}N_B|E_{2B}|^2], \tag{1f}$$

where $g_{1X} = 1 - s|E_{1X}|^2 - c|E_{2X}|^2$ and $g_{2X} = 1 - s|E_{2X}|^2 - c|E_{1X}|^2$. The coupling between the SRLs is modeled by a coupling amplitude $k_c$ and a coupling phase $\phi_c$. We assume that the travel time between the SRLs is of the same order as the cavity round-trip time, so that we can neglect any effects of a delay time. The two coupling sections to couple the light in and out of each SRL introduce an additional $\pi/2$ phase shift [28]. The light that is coupled from one SRL to the other passes through two such couplers. These two phase shifts add up to $\pi$, which explains the minus sign in front of the coupling term. No inhomogeneous broadening is taken into account as the experiments on such coupled SRLs reported (see, e.g., Ref. [8]) have been performed on InP-based multi-quantum-well SRLs, having a large uniformity over the device size with minimal well-width fluctuations. For simplicity, we use identical parameter values for SRL A and B. Unless mentioned otherwise, the parameter set used throughout this article is given in Table I.

We introduce a shorthand notation for the optical phase differences between the modes of different SRLs that are coupled to each other (the *inter*-SRL coupling):

$$\chi_1 = \phi_{1B} - \phi_{1A}, \tag{2a}$$

$$\chi_2 = \phi_{2B} - \phi_{2A} \tag{2b}$$

and for the optical phase differences between the modes of one SRL coupled to each other through backscattering (the *intra*-SRL coupling):

$$\psi_A = \phi_{2A} - \phi_{1A}, \tag{3a}$$

$$\psi_B = \phi_{2B} - \phi_{2B}, \tag{3b}$$

where $\phi_{nX} = \arg(E_{nX})$. The field at each side of the chip is given by $E_\alpha = E_{2A} + E_{2B}\exp(i\phi_c)$ and $E_\beta = E_{1A}\exp(i\phi_c) + E_{1B}$. The powers at both sides of the output waveguide are thus given by

$$P_\alpha = |E_{2A}|^2 + |E_{2B}|^2 + 2|E_{2A}||E_{2B}|\cos(\chi_2 + \phi_c), \tag{4a}$$

$$P_\beta = |E_{1A}|^2 + |E_{1B}|^2 + 2|E_{1A}||E_{1B}|\cos(\chi_1 - \phi_c). \tag{4b}$$

The optical phase differences that determine how the fields of both SRLs interfere at the outputs are $(\chi_2 + \phi_c)$ at the $\alpha$ port and $(\chi_1 - \phi_c)$ at the $\beta$ port. Note that this is different from the interference relation between the fields inside the SRLs. The optical phase differences determining the interference inside the rings have an offset of $\pi$ with respect to these values, being $(\chi_2 + \phi_c + \pi)$ and $(\chi_1 - \phi_c + \pi)$. This is due to the $\pi/2$ phase shifts introduced by the output couplers [28]. These phase shifts add up to $\pi$ when a field travels from one SRL to the other. But, they cancel each other when considering both fields in the output waveguide, outside the SRLs. Consequently, if $E_{1A}$ and $E_{1B}$ constructively interfere at the $\beta$ port, they must destructively interfere inside SRL B, and if $E_{2A}$ and $E_{2B}$ constructively interfere at the $\alpha$ port, they must destructively interfere inside SRL A, and vice versa.

The value of the coupling parameters $k_c$ and $\phi_c$ is *a priori* unknown. In Ref. [26], we have shown, however, that the dynamics of Eqs. (1) is $\pi$ periodic in $\phi_c$. Hence, we can limit ourselves to investigating $\phi_c \in [0,\pi]$. In the following sections, we will distinguish two qualitatively different cases, depending on the magnitude of the coupling $k_c$ compared to the backscattering $k$. In the first case of "weak coupling" (Sec. II), we will assume that $k_c$ is smaller or comparable to $k$ ($k_c/k \lesssim 1$). In the second case of "strong coupling" (Sec. III), we will assume that $k_c$ is much larger than $k$ ($k_c/k \gg 1$).

The coupling through a single waveguide changes the symmetry properties of the global system compared to those of a solitary SRL. Only one of the two counterpropagating modes of each SRL is fed through to the other SRL, and only one of the modes in each SRL receives input from the other SRL. When both SRLs are operating unidirectionally, this leads to globally symmetric and asymmetric states (see Fig. 2) with, respectively, equal and unequal power at the outputs in steady state. When both SRLs lase in opposite directions, there are two possibilities, depending on whether the dominant modes point outward [Fig. 2(a)], referred to as the $S_{out}$ state, or inward [Fig. 2(b)], referred to as the $S_{in}$ state. When both SRLs lase in the same direction, one SRL is injected by a high-power mode while the other SRL is injected by a low-power mode [see Figs. 2(c) and 2(d)], referred to as $A_{CCW}$ and $A_{CW}$, respectively. In this situation, the SRLs are experiencing different external inputs and will have different steady-state power levels.

It was noted in Ref. [8] that the single-waveguide-coupled SRLs can show dynamical behavior similar to an optically injected semiconductor laser. This can be understood by the directional bias that is introduced when the SRLs are operating unidirectionally. When the SRLs operate in an asymmetric state [see Fig. 2(c) or 2(d)], one of the SRLs is injected by

TABLE I. Summary of the physical meaning of the parameters in Eqs. (1) and their typical values used throughout this paper, unless stated otherwise.

| Symbol | Physical meaning | Simulation value |
|---|---|---|
| $\kappa$ | Field decay rate | 100 ns$^{-1}$ |
| $\gamma$ | Carrier decay rate | 0.2 ns$^{-1}$ |
| $\alpha$ | Linewidth enhancement factor | 3.5 |
| $s$ | Self-saturation coefficient | 0.005 |
| $c$ | Cross-saturation coefficient | 0.01 |
| $k$ | Backscattering parameter | 0.44 ns$^{-1}$ |
| $\phi_k$ | Backscattering phase | 1.5 |

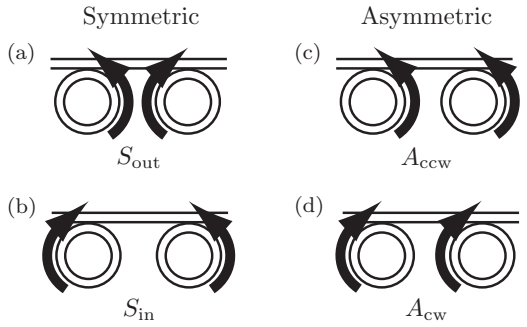


FIG. 2. Possible combinations in the single-waveguide-coupling configuration when the SRLs operate in the unidirectional regime. (a), (b) Symmetric states, equal output powers. $S_{out}$ has the high-power modes pointing outward, while $S_{in}$ has them pointing inward. (c), (d) Asymmetric states, unequal output powers. The $A_{CCW}$ ($A_{CW}$) asymmetry introduced by the coupling becomes apparent in cases (c) and (d), when both SRLs are lasing in the same direction.

a high-power mode, while the other SRL is injected by a low-power mode. In this state, the influence of the low-power mode that is fed through is negligible compared to the influence of the high-power mode that is fed through. Hence, the system behaves as if the coupling is unidirectional, just as in an optically injected laser system.

## II. WEAK COUPLING

We consider the coupling to be weak when the coupling amplitude between the SRLs is smaller than or comparable to the backscattering amplitude. This means that the coupling to the other SRL (the *inter*-SRL coupling) has to be weaker than or comparable to the reflective coupling between the counter-propagating modes inside each SRL (the *intra*-SRL coupling).

### A. Case 1: $\phi_c = 0$

We begin the investigation of weak coupling with a coupling amplitude that we have previously classified as such in Ref. [26], $k_c = 0.3k$, and a coupling phase of $\phi_c = 0$. The bifurcation diagram of the output power at the $\alpha$ port versus the bias current $\mu$ is shown in Fig. 3. The same bifurcation diagram for the internal mode amplitudes of each SRL and optical phase differences between the SRLs is shown in Fig. 4. The intra-SRL phase differences $\psi_A$ and $\psi_B$ are always very close to $\pi$ for all states and for all $\mu$, and are not shown. Taken together, these figures give us a clear picture of the different operating regimes.

At low currents, each SRL operates nearly bidirectionally, with almost equal powers in the counterpropagating modes. It can be seen in Fig. 4 that the outward modes ($E_{2A}$ and $E_{1B}$) have a slightly higher amplitude than the inward modes ($E_{1A}$ and $E_{2B}$). The clear nonzero power inside the SRLs is, however, in sharp contrast with the nearly zero output power shown in Fig. 3(a). This is because the phase differences $\chi_1$ and $\chi_2$ are very close to $\pi$, yielding destructive interference at the output ports, but constructive interference inside the SRLs.

At $\mu = 1.32$, a supercritical pitchfork bifurcation $PF_A$ occurs in which two stable asymmetric states $A_{CW}$ and $A_{CCW}$ are created and the bidirectional symmetric state becomes

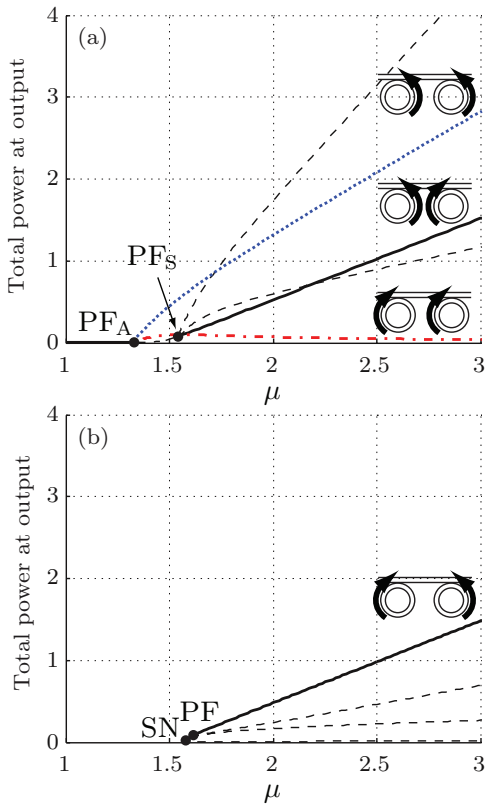


FIG. 3. (Color online) Bifurcation diagrams of fixed points of the total power at the $\alpha$ port versus the dimensionless bias current $\mu$. Panel (a) shows the bifurcation lines related to the asymmetric states ($A_{CCW}$, $A_{CW}$) and the symmetric $S_{out}$ solution, while panel (b) only depicts the bifurcation lines related to the symmetric $S_{in}$ solution. Solid, dotted, and dash-dotted lines indicate stable fixed points, while dashed lines indicate unstable fixed points. Blue-colored dotted branches belong to the $A_{CCW}$ solution and red-colored dash-dotted branches belong to the $A_{CW}$ solution (see also Fig. 4). Pitchfork (saddle-node) bifurcations are denoted by PF (SN). The bifurcation diagram for the total power at the $\beta$ port is identical. Parameter values: $k_c = 0.3k$, $\phi_c = 0$.

unstable. At $\mu = 1.55$, a subcritical pitchfork bifurcation $PF_S$ stabilizes the symmetric state $S_{out}$ again. From that point on, the two asymmetric states $A_{CW}$ and $A_{CCW}$ and the outward symmetric state $S_{out}$ are stable for all bias currents. The outward symmetric state $S_{out}$ is characterized by destructive interference at the outputs for all currents. But, above $\mu = 1.55$, the outward modes have a larger power than the inward modes. The destructive interference between such a high-power outward and a low-power inward mode does not yield zero power, as was the case for low currents. For the two asymmetric states $A_{CW}$ and $A_{CCW}$, the inter-SRL phase differences $\chi_1$ and $\chi_2$ are just above $\pi/2$ or just below $3\pi/2$, respectively. This means that the maximum output power of the asymmetric states is generated by the interference of the two high-power modes of both SRLs with a relative phase difference of approximately $\pi/2$. Note that if this phase difference would be zero, the maximum output power would be twice as high.

From $\mu = 1.6$ on, we also find the inward symmetric state $S_{in}$, but it is located on a separate solution branch [see Fig. 3(b)]. For increasing $\mu$, it is created in a subcritical pitchfork bifurcation PF succeeding a saddle-node bifurcation

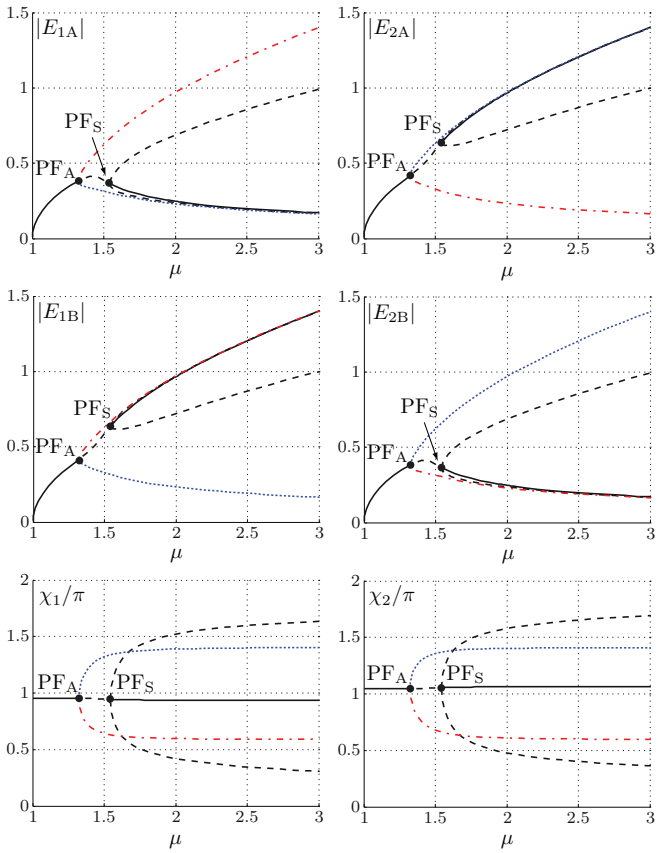


FIG. 4. (Color online) Bifurcation diagrams of intra-SRL mode amplitudes ($|E_{1A}|$, $|E_{2A}|$, $|E_{1B}|$, $|E_{2B}|$, see Fig. 1) and inter-SRL optical phase differences ($\chi_1$, $\chi_2$). Solid, dotted, and dash-dotted lines indicate stable fixed points, while dashed lines indicate unstable fixed points. Blue-colored dotted branches belong to the $A_{\mathrm{CCW}}$ solution and red-colored dash-dotted branches belong to the $A_{\mathrm{CW}}$ solution (see also Fig. 3). Pitchfork bifurcations are denoted by PF. Parameter values: $k_c = 0.3k$, $\phi_c = 0$.

SN. The pitchfork bifurcation stabilizes one of the two unstable states created in the preceding saddle-node bifurcation. Just as the outward symmetric state $S_{\mathrm{out}}$, it is characterized by destructive interference at the outputs and constructive interference inside the SRL ($\chi_1 \approx \chi_2 \approx \pi$), yielding almost the same output power levels as the $S_{\mathrm{out}}$ state. The inward symmetric state $S_{\mathrm{in}}$ also remains stable for all larger bias currents.

A common trait of the previous bifurcation diagrams is the absence of periodic solutions. Weak coupling and a coupling phase $\phi_c \approx 0$ prove to have a stabilizing influence in the sense that there exists no oscillatory regime, even at parameter values for which the solitary SRLs exhibit oscillatory behavior (alternate oscillations). In an oscillatory SRL it has also been shown experimentally that one can avoid oscillations by appropriately changing the coupling phase $\phi_k$ [3]. For a complete bifurcation analysis of the solitary SRL, we refer to Refs. [27,29].

### B. Case 2: $\phi_c = \pi/2$

As a second case, we keep the same coupling amplitude $k_c = 0.3k$, but change the coupling phase $\phi_c$ to $\pi/2$. The four different states are located on four different solution

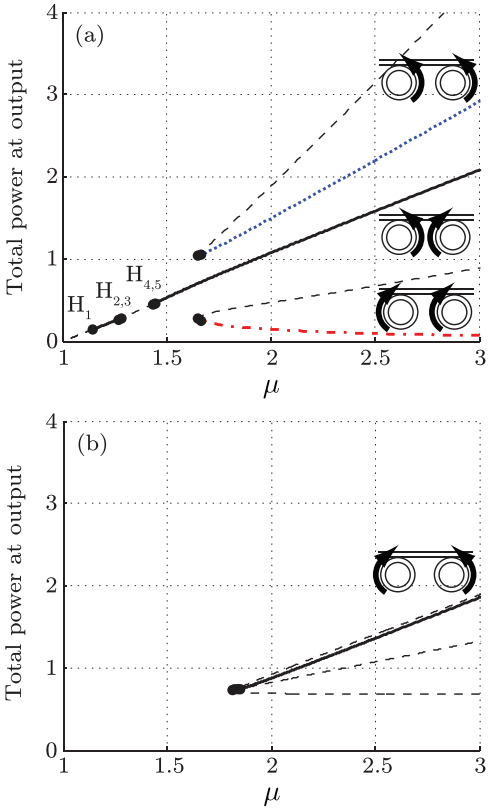


FIG. 5. (Color online) Bifurcation diagrams with conventions as in Fig. 3. In the regions delimited by the Hopf bifurcations $H_1$ to $H_5$, there exists at least one stable limit cycle. Parameter values: $k_c = 0.3k$, $\phi_c = \pi/2$.

branches (shown in Fig. 5). Like the case $\phi_c = 0$, the only stable solution at low currents is the outward symmetric state $S_{\mathrm{out}}$, or oscillatory solutions emanating from this state [related to the Hopf bifurcations $H_1$ to $H_5$ in Fig. 5(a)]. In $S_{\mathrm{out}}$, all phase variables are close to $\pi$ again. Since $\phi_c = \pi/2$, this means that the phase difference inside the SRLs and at the outputs are $\pm\pi/2$, resulting in higher-power levels at the outputs than for the previous case where $\phi_c = 0$. The steady-state bifurcates into limit cycles through Hopf bifurcations for currents approximately in the range 1.28 to 1.45, and currents below 1.14. Hopf bifurcations occur at $\mu =$ 1.14 ($H_1$), 1.28 ($H_2$), 1.29 ($H_3$), 1.43 ($H_4$), and 1.45 ($H_5$), corresponding to three different limit cycles. The bifurcations $H_1$ to $H_4$ are all supercritical, while $H_5$ is subcritical. The oscillation regime for currents below $H_1$ is characterized by a frequency very close to the relaxation oscillation frequency, as shown in Fig. 6(a) for $\mu = 1.1$ ($f_{\mathrm{R}} \approx 0.32$ GHz at $\mu = 1.1$). Note that these relaxation oscillations in SRL A and SRL B are exactly in antiphase between the two lasers. The oscillation regime between $H_2$ and $H_5$ is characterized by two slower frequencies very close to the alternate oscillation frequency. In both of these limit cycles, each SRL exhibits alternate oscillations within one laser. For the limit cycle shown in Fig. 6(b), the codirectional modes in both SRLs [both CW (CCW) modes in each SRL] are oscillating in antiphase, and $P_\alpha$ and $P_\beta$ oscillate in phase. This limit cycle is related to the $H_3$ and the $H_5$ bifurcation. In the other limit cycle related to $H_2$ and $H_4$ (not shown), the codirectional modes in both SRLs

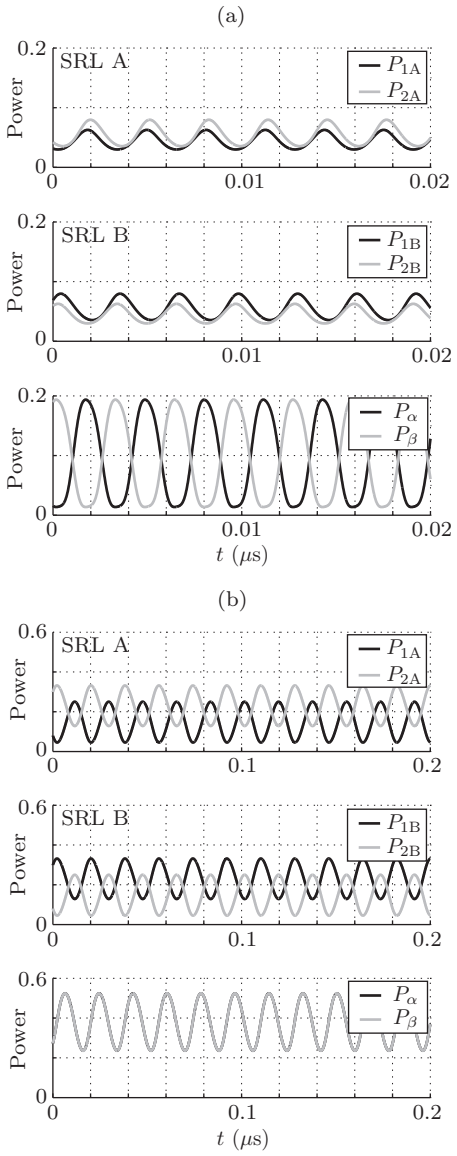


FIG. 6. Oscillatory solutions from Fig. 5. From top to bottom: power of the modes in SRL A ($P_{1A} = |E_{1A}|^2$ and $P_{2A} = |E_{2A}|^2$), power of the modes in SRL B ($P_{1B} = |E_{1B}|^2$ and $P_{2B} = |E_{2B}|^2$), and power at the outputs $\alpha$ and $\beta$ ($P_\alpha$ and $P_\beta$). (a) $\mu = 1.1$ (related to $H_1$). (b) $\mu = 1.38$ (limit cycles related to $H_3$ and $H_5$). Parameter values: $k_c = 0.3k$, $\phi_c = \pi/2$.

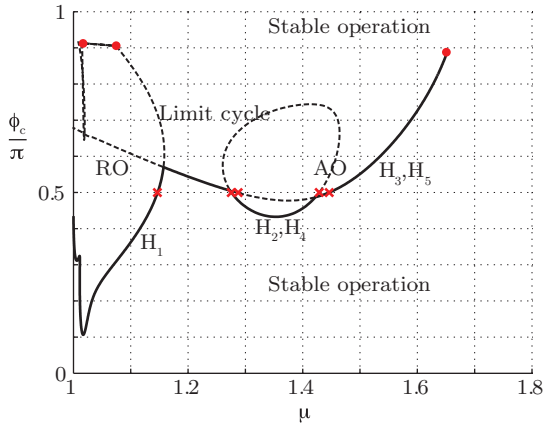


FIG. 7. (Color online) Two-parameter continuation in $(\mu,\phi_c)$ of the Hopf bifurcations responsible for the oscillatory regimes in Fig. 5. They are defined as $H_1$ to $H_5$ for increasing $\mu$ in Fig. 5. The solid (dashed) line indicates a Hopf bifurcation of a stable (unstable) structure. RO stands for relaxation oscillations and AO stands for alternate oscillations. The red crosses indicate the bifurcations points of Fig. 5, where $\phi_c = \pi/2$. The red circles are branch points. Parameter values: $k_c = 0.3k$.

are oscillating in phase, and $P_\alpha$ and $P_\beta$ oscillate in antiphase. This limit cycle is related to the $H_2$ and the $H_4$ bifurcations. For $\mu$ between $H_2$ and $H_5$, at least one of these two limit cycles is stable, and for a small range of currents they are both stable.

In Fig. 7, we show the two-parameter continuation of the Hopf bifurcations $H_1$ to $H_5$ in $(\mu,\phi_c)$. This figure shows that the value of $\phi_c$ plays an important role in these oscillatory regimes. The red crosses show the bifurcation points corresponding to $\phi_c = \pi/2$, as in Fig. 5. Below the solid black line and above the red circles, which are branch points, the $S_{out}$ state is stable. The exact bifurcation structure through which $S_{out}$ turns stable above the branching points is not fully understood and not the main focus of the current article. Our aim is only to prove that there exists a whole region of oscillatory instabilities for $\phi_c$ close to and higher than $\pi/2$, while for $\phi_c \approx 0$ oscillatory solutions are suppressed.

The bifurcation diagram of the inward symmetric state $S_{in}$ is shown in Fig. 5(b) for $\phi_c = \pi/2$. It undergoes a series of very closely spaced bifurcations for increasing current (respectively, saddle node, Hopf, pitchfork, Hopf) and turns into a stable state through the last of these bifurcations (subcritical Hopf) at $\mu = 1.85$. Again, $\chi_1$ and $\chi_2$ are close to $\pi$, but since $\phi_c = \pi/2$ the interference is not destructive, yielding higher output powers than the $\phi_c = 0$ case.

The asymmetric states $A_{CW,CCW}$ are no longer found on the same branch as the outward symmetric state $S_{out}$. They are now each generated by a saddle-node bifurcation at $\mu = 1.66$ that creates two unstable states, closely followed by a Hopf bifurcation at $\mu = 1.67$ that stabilizes one of the created states. In this state, the values of $\chi_1$ and $\chi_2$ are also close to $\pi$. Taking into account $\phi_c = \pi/2$ leads to power levels similar to the $\phi_c = 0$ case. An important difference between the two cases is the bias current at which the asymmetric states are created. In the $\phi_c = 0$ case they are created at $\mu = 1.32$ [$PF_A$ in Fig. 3(a)], compared to $\mu = 1.67$ for the $\phi_c = \pi/2$ case. This confirms that also here $\phi_c$ close to zero has a stabilizing influence, while $\phi_c$ close to $\pi/2$ has a destabilizing influence. Note that the value $\mu = 1.32$ is even lower than the minimum current to obtain unidirectional operation in solitary SRLs ($\mu = 1.58$ for these parameter values), which was also noticed in Ref. [6].

When adding noise to the model, we find that all four states ($A_{CW}$, $A_{CCW}$, $S_{out}$, $S_{in}$) are stable. In the experiment reported in Ref. [8], the three states $A_{CW}$, $A_{CCW}$, $S_{out}$ were observed, although the state $S_{in}$ was not. The lasers A and B operated at approximately 1560 nm and their free running lasing wavelength differed by 2–3 nm. Since the free spectral range was 0.41 nm, locking could be achieved in the asymmetric states by aligning the frequency combs through an offset in bias current. Locking could not be achieved for $S_{out}$, even

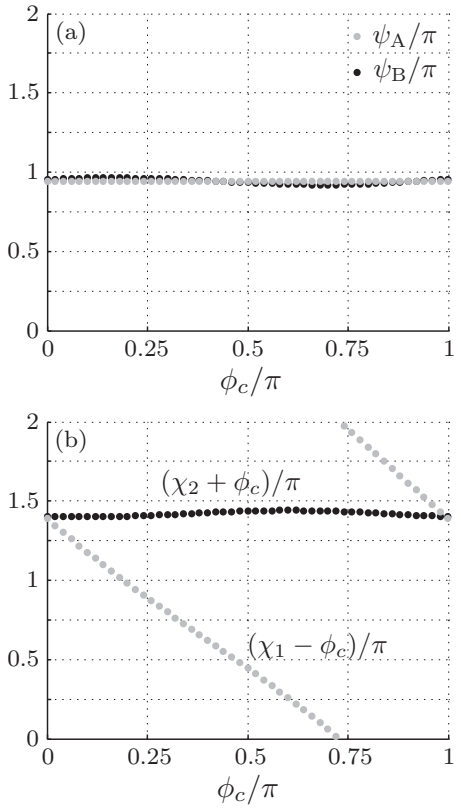


FIG. 8. Numerical simulation of Eqs. (1) depicting the intra-SRL ($\psi_{A,B}$) and inter-SRL ($\chi_{1,2}$) phase differences in the asymmetric state $A_{CCW}$ as a function of the coupling phase $\phi_c$. The intra-SRL phase differences $\psi_A$ and $\psi_B$ are relatively insensitive to variations of $\phi_c$. The inter-SRL phase difference between the high-power CCW modes $\chi_2+\phi_c$ is kept fixed, while the phase difference between the low-power CW modes $\chi_1-\phi_c$ spans the whole $[0,2\pi]$ interval for $\phi_c$ going from 0 to $\pi$. Parameter values: $\mu=2$, $k_c=0.3k$.

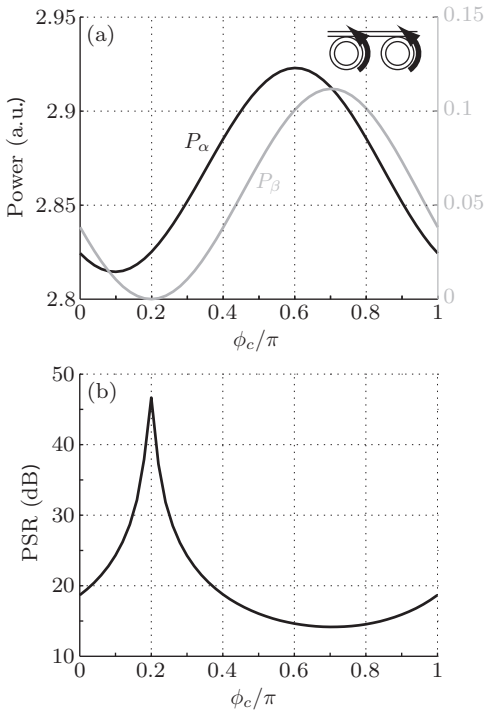


FIG. 9. Numerical simulations of Eqs. (1). (a) Steady-state power levels at the $\alpha$ port (left axis, black) and $\beta$ port (right axis, red) of the $A_{CCW}$ state as a function of the coupling phase $\phi_c$. The minimum value of $P_\beta$ is $6\times10^{-5}$. (b) Power suppression ratio (PSR) of the $A_{CCW}$ state as a function of the coupling phase $\phi_c$. Parameter values: $k_c=0.3k$, $\mu=3$.

though their frequency combs were aligned. SRL A and B lased outward at their own free-running wavelength, subject to a nonresonant injection from low-power mode of the other laser. The state $S_{in}$ is characterized by injection from the high-power mode of the other laser. Although its existence is predicted by the modeling for identical SRLs, this state was not observed in the experiment where the parameters of the SRLs slightly differ. This might be understood because the high-power modes from A and B simultaneously enforce locking at different wavelengths due to the mismatch.

### C. Power suppression ratio (PSR)

When comparing the asymmetric $A_{CW}$ ($A_{CCW}$) states in Figs. 3(a) and 5(a), we noticed that the power levels at the $\beta$ ($\alpha$) port are comparable, but that the power levels at the $\alpha$ ($\beta$) port are higher for the $\phi_c=\pi/2$ than for the $\phi_c=0$ case. The underlying reason for this is that the inter-SRL phase difference between the high-power modes remains constant when changing $\phi_c$, while the phase difference between the low-power modes changes. We illustrate this in Fig. 8. We choose a constant current $\mu=2$, such that the asymmetric state is stable for all $\phi_c$, and vary $\phi_c$ (the results are qualitatively the same for other values of $\mu$ at which the asymmetric state is stable for all $\phi_c$). In the $A_{CCW}$ state, the high-power modes are $E_{2A}$ and $E_{2B}$, while the low-power modes are $E_{1A}$ and $E_{1B}$. The phase difference between the high-power modes at the output is hence $\chi_2+\phi_c$, and the phase difference between the low-power modes is $\chi_1-\phi_c$. The intra-SRL phase differences $\psi_A$ and $\psi_B$ do not significantly change with $\phi_c$, and are close to $\pi$ [see Fig. 8(a)]. The phase difference between the high-power modes $\chi_2+\phi_c$ is also insensitive to $\phi_c$. However, the phase difference between the low-power modes $\chi_1-\phi_c$ covers the whole $[0,2\pi]$ interval for $\phi_c$ ranging from 0 to $\pi$ [see Fig. 8(b)].

As a result, the relative amount of variation of the power level as a function of $\phi_c$ is very different at the output ports $P_\alpha$ and $P_\beta$, which are given by Eqs. (4). This is illustrated in Fig. 9(a). In this figure, we have chosen $\mu=3$ to demonstrate that these results are robust to reasonable parameter variations. It is clear that while $P_\alpha$ only varies a few percent, $P_\beta$ ranges from 0.11 to practically zero ($6\times10^{-5}$). This minimum occurs at the point where the phase difference between the low-power modes at the output port $\chi_1-\phi_c$ is equal to $\pi$, yielding destructive interference (this happens when $\phi_c=0.2\pi$, see Fig. 8). Naturally, this causes a sharp peak of 47 dB in the power suppression ratio $P_\alpha/P_\beta$, as shown in Fig. 9(b). The solitary SRL has a PSR of 18 dB at $\mu=3$ (at the same parameter values). So, using two coupled SRLs seems to be advantageous from the viewpoint of PSR. However, since we need to bias two SRLs at $\mu=3$ to achieve the PSR of 47 dB, it is better to compare it with a solitary SRL biased at twice the current $\mu=6$, which has a PSR of 26 dB. This comparison still shows an improved PSR for the coupled case.

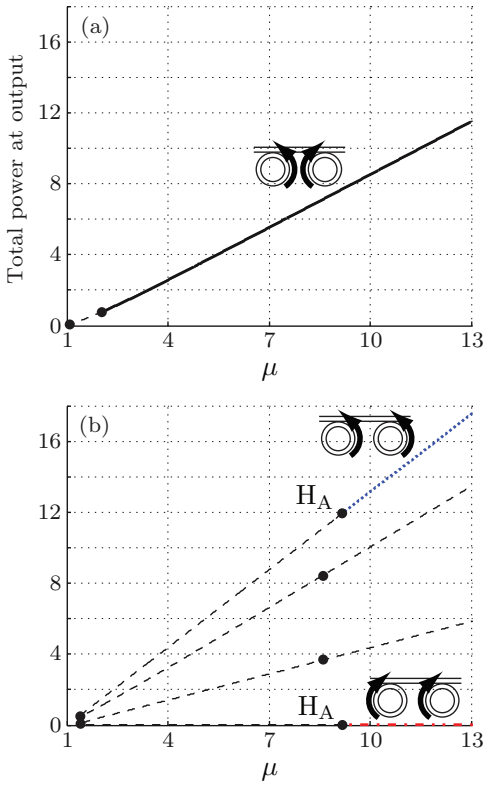


FIG. 10. (Color online) Bifurcation diagrams with conventions as in Fig. 3. Parameter values: $k_c = 20k$, $\phi_c = 0$.

Nevertheless, the practical advantage of the higher PSR of single-waveguide-coupled SRLs (as also reported in Ref. [6]) can be argued since it arises rather due to a decrease of the low-power level, than top an increase in the high-power level.

## III. STRONG COUPLING

We now set $k_c = 20k$, such that the inter-SRL coupling is significantly larger than the intra-SRL coupling. For, $\phi_c = 0$, the bifurcation diagrams of all steady states are shown in Fig. 10. Figure 10(a) shows the bifurcation diagram of $S_{\text{out}}$. A very notable fact is that the symmetric $S_{\text{out}}$ state is stable at far lower currents (from $\mu = 2.04$ on) than the $A_{\text{CW,CCW}}$ states (from $\mu = 9.18$ on). $S_{\text{out}}$ is also stable for currents close to threshold, from $\mu = 1$ up to $\mu = 1.006$, where it is destabilized in a subcritical Hopf bifurcation. This Hopf bifurcation is actually the same as $H_1$ in Fig. 5(a) at $\mu = 1.14$, and is related to the excitation of relaxation oscillations. Such destabilization through a Hopf bifurcation now also occurs at coupling phases $\phi_c$ near zero for these higher values of $k_c$. The $S_{\text{in}}$ state is no longer observed for these high coupling values in the considered current range, as can be expected due to the destabilizing influence of the coupling on this state (see Fig. 2).

The bifurcation diagram of the asymmetric states is shown in Fig. 10(b). As mentioned before, the asymmetric states are only stable for current values above $\mu = 9.18$. The reason for this is the existence of a supercritical Hopf bifurcation $H_{\text{A}}$ at $\mu = 9.18$. For currents lower than this, the asymmetric states (needed for optical memory operation) are unstable or simply do not exist. It is only at relatively high-bias currents ($\mu = 9.18$) that the asymmetric states are stabilized, and they

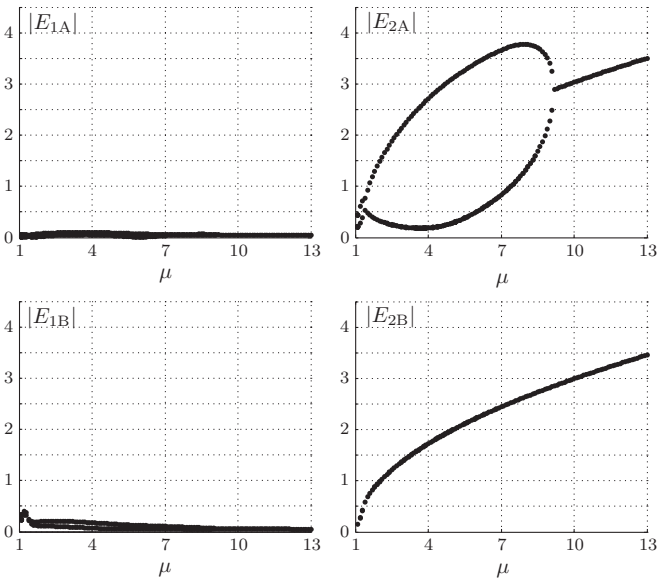


FIG. 11. Orbit diagram depicting local extrema constructed by numerical simulation of Eq. (1). The orbit diagram was initialized in the asymmetric state $A_{\text{CCW}}$ at $\mu = 20$ before decreasing the current to $\mu = 1$. Parameter values: $k_c = 20k$, $\phi_c = 0$.

remain stable for all higher current values. The limit cycle related to this Hopf bifurcation has a very different amplitude in SRL A and SRL B. Figure 11 shows an orbit diagram depicting all local extrema for the different fields of the SRL in a region where the Hopf bifurcation occurs. It can be seen that the oscillation amplitude of the limit cycle is very large in one SRL, while being almost negligible in the other.

The frequency of this limit cycle is of the same order but slightly larger than the relaxation oscillation frequency of the solitary SRLs. For example, at $\mu = 8$ the relaxation oscillation frequency is 2.66 GHz and the frequency of the limit cycle is 3.57 GHz. Hence, this scenario is very similar to the case of an optically injected laser [30–33]. One SRL acts as the master laser (negligible oscillation amplitude) and drives the second SRL (large oscillation amplitude) into relaxation oscillations. However, the coupling in this system is bidirectional, as opposed to the unidirectional coupling from master to slave in an optically injected laser. The similarity stems from the nature of the modes that are coupled to the other SRL. In the asymmetric state, a high-power mode is fed through in one direction, while a low-power mode is fed through in the other direction (see Fig. 2), producing a bias in the directionality of the coupling.

The bifurcation diagram of the asymmetric states for $\phi_c = \pi/2$ is the same as in Fig. 10(b), although the power level of the low-power side is again higher for $\phi_c = \pi/2$ than for $\phi_c = 0$. Figure 12(a) is the two-parameter continuation of the Hopf bifurcation $H_{\text{A}}$ in $(\mu,\phi_c)$, and it shows that the location of $H_{\text{A}}$ is insensitive to the value of the $\phi_c$.[1] However, the current value at which the $H_{\text{A}}$ occurs does drastically change with varying $k_c$. This is shown by the two-parameter continuation in $(\mu,k_c)$ in Fig. 12(b). The solid line represents

[1]Varying $\phi_c$ roughly moves $H_{\text{A}}$ between $\mu = 9.17$ and 9.19 [not visible in Fig. 12(a)].

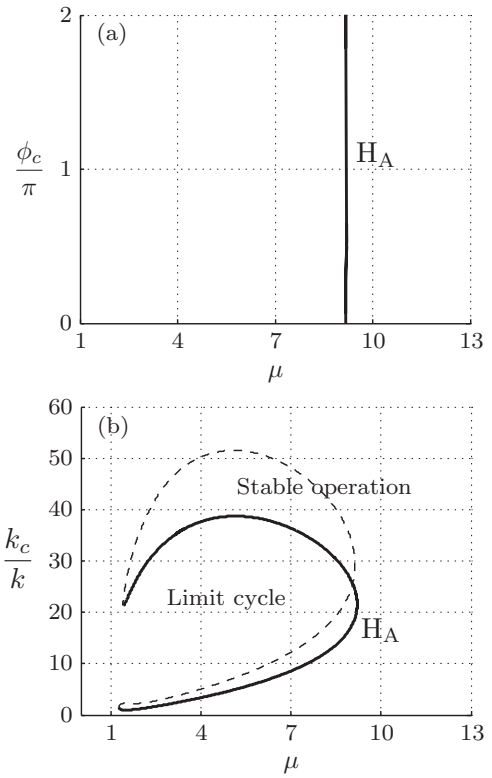


FIG. 12. (a) Two-parameter continuation in $(\mu,\phi_c)$ of $H_A$ in Fig. 10. Parameter values: $k_c = 20k$. (b) Two-parameter continuation in $(\mu,k_c)$ of $H_A$ in Fig. 10. The solid (dashed) line indicates a Hopf bifurcation of a stable (unstable) structure. Note that the current $\mu_H$ at which the bifurcation takes place hardly changes with the coupling phase $\phi_c$, but drastically changes with $k_c$. Parameter values: $\phi_c = 0$.

a Hopf bifurcation of a stable structure ($H_A$), while the dashed line represents a Hopf bifurcation of an unstable structure [located on the unstable branch in Fig. 10(b)]. For increasing $k_c$, $H_A$ folds back on itself. This means that for higher $k_c$, two Hopf bifurcations will occur that move toward each other before completely disappearing.

Above $k_c/k \approx 40$, the asymmetric state is no longer destabilized by $H_A$, and stable operation is obtained for all currents above the saddle-node bifurcation. We illustrate this in Fig. 13(a), which is the bifurcation diagram of the asymmetric state for $k_c = 100k$. The saddle-node bifurcation $S_A$ is located at $\mu_S = 1.61$ and now determines at which current value stable operation in the asymmetric state becomes possible. There is a substantial influence of $\phi_c$ on the exact location of this bifurcation, shown in Fig. 13(b). As we continue $S_A$ in $(\mu,\phi_c)$, we see that $\mu_S$ varies between 1.47 and 2.69, depending on the value of $\phi_c$. When the coupling waveguide length is such that it corresponds to constructive ($\phi_c = \pi$) or destructive ($\phi_c = 0$) interference between the coupled fields, the asymmetric state is stable for significantly lower-bias currents.[2] Once again, coupling phases $\phi_c$ close to $\pi/2$ shift the stability of steady-state solutions to higher-bias currents.

[2]Note that the two couplers each introduce a $\pi/2$ phase shift that add up with $\phi_c$.

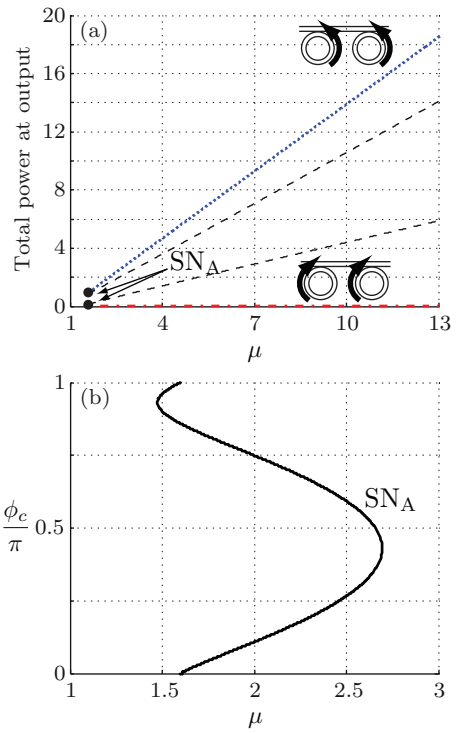


FIG. 13. (Color online) (a) Bifurcation diagram with conventions as in Fig. 3. Parameter values: $k_c = 100k$, $\phi_c = 0$. (b) Two-parameter continuation in $(\mu,\phi_c)$ of $S_A$ in (a). Parameter values: $k_c = 100k$.

Some of the important changes in the dynamical regimes take place at relatively high values of the parameters. This raises the question as to whether these high-parameter values are physically attainable in experimental setups. Concerning the bias current $\mu$, its values can be mapped on the device bias current $I$ using the values of the threshold current $I_{thr}$ and the transparency current $I_{tr}$. These are identified with the values $\mu = 1$ (threshold) and $\mu = 0$ (transparency), respectively, yielding the following relation for the bias current $I$:

$$I = (I_{thr} - I_{tr})\mu + I_{tr}. \tag{5}$$

A value of $\mu \approx 9$ is an experimentally attainable value in semiconductor ring laser devices. For example, the semiconductor ring lasers used in Ref. [25] have a threshold current $I_{thr} = 35$ mA and a transparency current $I_{tr} = 25$ mA, such that a normalized current $\mu = 9$ corresponds to an actual driving current $I = 115$ mA. These ring laser devices have been exposed to even higher currents without being damaged.

The modeling in the paper of Hill *et al.* assumed $k_c \gg k$, which according to our analysis should excite relaxation oscillations. Since the coupling from the rings to the coupling waveguide was only 1.5% [1], and since the small size of the SRLs increases the amount of backscattering, we suspect that they rather operated in the low-coupling limit $k_c \ll k$. This would explain the stability of the asymmetric states $A_{CW,CCW}$, which is needed for stable flip-flop functionality. In this weak-coupling regime, where relaxation oscillations are not excited, there seems to be an optimal operating regime for functionality as an optical memory, at $\phi_c \approx 0$. For these parameters, there is a low-bias current range in which the functionality would not be disturbed by the existence of $S_{out}$ since it is unstable. For

$1.32 < \mu < 1.55$ (between $PF_A$ and $PF_S$ in Fig. 3), $A_{CW,CCW}$ are the only stable states. However, in this range, the maximum power suppression ratio that can be achieved between the output ports is 7.3 dB at $\mu = 1.54$. Even though this current value is lower than the bias current at which the unidirectional regime starts in solitary SRLs ($\mu = 1.58$), two SRLs have to be biased at $\mu = 1.54$. A better comparison is given by biasing a solitary SRL at $\mu = 3$, which yields a power suppression ratio of approximately 18 dB. So, even in this optimal regime (without the excitation of relaxation oscillations and the existence of a stable symmetric state $S_{out}$), using coupled SRLs does not seem to have an advantage over solitary SRLs.

## IV. DISCUSSION

In this article, we have investigated SRLs that are coupled by a single bus waveguide. We used an amplitude-phase description of the coupling, giving rise to two new parameters: the field coupling strength $k_c$ and the accumulated optical phase $\phi_c$ when traveling from one SRL to the other. When both SRLs are operating unidirectionally, this can lead to globally symmetric and asymmetric states, with respectively equal and unequal power at the outputs (see Fig. 2). The asymmetric states $A_{CW,CCW}$ have both SRLs lasing in the same direction, respectively: the clockwise and the counterclockwise directions. The symmetric states $S_{in,out}$ have both SRLs lasing in the opposite direction, both respectively lasing inward and outward.

Weak coupling can have a stabilizing influence on the SRL operating regimes. If the coupling phase $\phi_c$ is near zero, oscillatory regimes are completely suppressed in the weakly coupled SRLs, even at parameter ranges where solitary SRLs exhibit alternate oscillations. The power level of the high-power port in the $A_{CW,CCW}$ states is independent of $\phi_c$, but the power level of the low-power port is not. The reason for this is that the high-power modes of each SRL impose a fixed inter-SRL phase relationship very close to $-\pi/2$, whatever the value of $\phi_c$. The inter-SRL phase difference between the low-power modes is therefore slaved and spans the whole $[0,2\pi]$ interval for $\phi_c$ going from 0 to $\pi$. The interference of the low-power modes of each SRL will hence be destructive or constructive depending on the value of $\phi_c$, yielding different power suppression ratios.

A strong coupling destabilizes the asymmetric states $A_{CW,CCW}$ due to the excitation of relaxation oscillations up to currents almost 10 times the threshold current, regardless of the value of $\phi_c$. Relatively low-coupling strengths are sufficient to trigger these relaxation oscillations. They occur for coupling amplitudes $k_c$ ranging from $O(k)$ to $O(40k)$, where $k$ is the backscattering amplitude. For coupling values larger than $40k$, the asymmetric states are stabilized again. This is similar to the behavior of optically injected lasers, where relaxation oscillations are first excited for low to moderate injection powers and subsequently damped for higher injection powers. This similarity is emphasized by the fact that in this regime the mode powers in one SRL are almost constant, while the mode powers in the other SRL are oscillating near the relaxation oscillation frequency. So, although the coupling in our system is bidirectional, the SRLs behave very similar to an optically injected laser system. For this range of coupling amplitudes, the coupled SRLs will preferably reside in the $S_{out}$ state, which is always stable for much lower bias currents than the $A_{CW,CCW}$ states.

A generally observed feature is that coupling phases $\phi_c$ close to $\pi/2$ promote instabilities, in the sense of oscillatory solutions or shifting the stability of steady-state solutions to higher-bias currents. For instance, at weak-coupling amplitudes, oscillatory solutions (related to either relaxation oscillations or alternate oscillations) were possible for $\phi_c$ close to $\pi/2$, and the current at which the asymmetric states $A_{CW,CCW}$ become stable are notably larger for $\phi_c$ close to $\pi/2$ (1.66 for $\phi_c = \pi/2$ versus 1.32 for $\phi_c = 0$). For very strong coupling, the asymmetric states turn stable at markedly higher-bias currents when $\phi_c$ is close to $\pi/2$. Note that this is in correspondence with the results on coupled excitable SRLs in Ref. [26], in which the ability to excite a response in the second SRL also required a coupling phase $\phi_c$ close to $\pi/2$.

Regarding optical memory operation proposed using two SRLs coupled by a single waveguide, our analysis indicates that there is no real advantage for bistable memory operation compared to using a solitary SRL. The increased power suppression ratio is mainly due to the destructive interference of the SRL fields at the low-power port, and its usefulness can hence be argued. Moreover, coupling of the same order as the backscattering can excite relaxation oscillations, resulting in a periodic rather than a stable output power level. Finally, there will often exist multistability between the asymmetric states $A_{CW,CCW}$ used for optical memory operation and the outward symmetric state $S_{out}$. All these factors are detrimental for bistable optical memory operation, and indicate that solitary SRLs are better suited for serving as an all-optical memory. One could on the one hand also argue that the coexistence of multiple stable states (the asymmetric and outward symmetric states) could be potentially interesting to store more than one bit of information in a single optical memory unit. However, on the other hand, accurately controlling switching between these stable states would probably require a more complicated setup (e.g., additional waveguides) and control scheme.

## ACKNOWLEDGMENT

This research was supported by the Research Foundation-Flanders (FWO) and the Belgian Science Policy Office (BelSPO) under Grant No. IAP 7-35.

[1] M. T. Hill, H. J. S. Dorren, T. de Vries, X. J. M. Leijtens, J. H. den Besten, B. Smalbrugge, Y. S. Oei, H. Binsma, G. D. Khoe, and M. K. Smit, Nature (London) **432**, 206 (2004).

[2] M. Sorel, P. Laybourn, G. Giuliani, and S. Donati, Appl. Phys. Lett. **80**, 3051 (2002).

[3] L. Gelens, S. Beri, G. Van der Sande, G. Mezosi, M. Sorel, J. Danckaert, and G. Verschaffelt, Phys. Rev. Lett. **102**, 193904 (2009).

[4] L. Liu, R. Kumar, K. Huybreghts, T. Spuesens, G. Roelkens, E. Geluk, T. de Vries, P. Regreny, D. Van Thourhout, R. Baets, and G. Morthier, Nat. Photonics **4**, 182 (2010).

[5] S. Ishii, A. Nakagawa, and T. Baba, IEEE J. Sel. Top. Quantum Electron. **12**, 71 (2006).
[6] Y. De Koninck, K. Huybrechts, G. Van der Sande, J. Danckaert, R. Baets, and G. Morthier, in *2009 IEEE LEOS Annual Meeting Conference Proceedings, Belek-Antalya, Turkey* (IEEE, Washington, DC, 2009), Vols. 1 and 2, pp. 503–504.
[7] J. D. Lin, Y. Z. Huang, Y. D. Yang, Q. F. Yao, X. M. Lv, J. L. Xiao, and Y. Du, Opt. Lett. **36**, 3515 (2011).
[8] W. Coomans, L. Gelens, G. Van der Sande, G. Mezosi, M. Sorel, J. Danckaert, and G. Verschaffelt, Appl. Phys. Lett. **100**, 251114 (2012).
[9] T. Krauss, P. J. R. Laybourn, and J. Roberts, Electron. Lett. **26**, 2095 (1990).
[10] J. Mulet, C. Masoller, and C. R. Mirasso, Phys. Rev. A **65**, 063815 (2002).
[11] H. J. Wünsche, S. Bauer, J. Kreissl, O. Ushakov, N. Korneyev, F. Henneberger, E. Wille, H. Erzgräber, M. Peil, W. Elsäßer, and I. Fischer, Phys. Rev. Lett. **94**, 163901 (2005).
[12] C. Bonatto, B. Kelleher, G. Huyet, and S. P. Hegarty, Phys. Rev. E **85**, 026205 (2012).
[13] H. Erzgräber, S. Wieczorek, and B. Krauskopf, Phys. Rev. E **81**, 056201 (2010).
[14] M. Brunstein, T. J. Karle, I. Sagnes, F. Raineri, J. Bloch, Y. Halioua, G. Beaudoin, L. L. Gratiet, J. A. Levenson, and A. M. Yacomotti, Appl. Phys. Lett. **99**, 111101 (2011).
[15] H. Erzgräber, S. Wieczorek, and B. Krauskopf, Phys. Rev. E **78**, 066201 (2008).
[16] G. Fasching, C. Deutsch, A. Benz, A. Andrews, P. Klang, R. Zobl, W. Schrenk, G. Strasser, P. Ragulis, V. Tamosiunas, and K. Unterrainer, Opt. Express **17**, 20321 (2009).
[17] M. Liertzer, L. Ge, A. Cerjan, A. D. Stone, H. E. Türeci, and S. Rotter, Phys. Rev. Lett. **108**, 173901 (2012).
[18] M. Smit, J. van der Tol, and M. Hill, Laser Photon. Rev. **6**, 1 (2012).
[19] A. Hohl, A. Gavrielides, T. Erneux, and V. Kovanis, Phys. Rev. Lett. **78**, 4745 (1997).
[20] J. R. Terry, K. S. Thornburg, Jr., D. J. Deshazer, G. D. Vanwiggeren, S. Zhu, P. Ashwin, and R. Roy, Phys. Rev. E **59**, 4036 (1999).
[21] S. Riyopoulos, Phys. Rev. A **66**, 053820 (2002).
[22] F. Rogister and R. Roy, Phys. Rev. Lett. **98**, 104101 (2007).
[23] R. Vicente, I. Fischer, and C. R. Mirasso, Phys. Rev. E **78**, 066202 (2008).
[24] G. Van der Sande, M. C. Soriano, I. Fischer, and C. R. Mirasso, Phys. Rev. E **77**, 055202 (2008).
[25] L. Gelens, L. Mashal, S. Beri, W. Coomans, G. Van der Sande, J. Danckaert, and G. Verschaffelt, Phys. Rev. A **82**, 063841 (2010).
[26] W. Coomans, L. Gelens, S. Beri, J. Danckaert, and G. Van der Sande, Phys. Rev. E **84**, 036209 (2011).
[27] L. Gelens, G. Van der Sande, S. Beri, and J. Danckaert, Phys. Rev. E **79**, 016213 (2009).
[28] D. Marcuse, Bell Syst. Tech. J. **50**, 1791 (1971).
[29] L. Gelens, S. Beri, L. Mashall, G. Van der Sande, J. Danckaert, and G. Verschaffelt, Eur. Phys. J. D **58**, 197 (2010).
[30] V. Kovanis, T. Erneux, and A. Gavrielides, Opt. Commun. **159**, 177 (1999).
[31] S. Wieczorek, B. Krauskopf, and D. Lenstra, Opt. Commun. **172**, 279 (1999).
[32] S. Wieczorek, B. Krauskopf, T. B. Simpson, and D. Lenstra, Phys. Rep. **416**, 1 (2005).
[33] W. Coomans, S. Beri, G. Van der Sande, L. Gelens, and J. Danckaert, Phys. Rev. A **81**, 033802 (2010).